BBA - Biomembranes 1865 (2023) 184179

Contents lists available at ScienceDirect

BBA - Biomembranes

journal homepage: www.elsevier.com/locate/bbamem

Shaping membrane interfaces in lipid vesicles mimicking the cytoplasmic leaflet of myelin through variation of cholesterol and myelin basic protein contents

Jennica Träger [a,b], Annette Meister [b,c], Gerd Hause [d], George Harauz [e], Dariush Hinderberger [a,b,*]

[a] Institute of Chemistry, Physical Chemistry – Complex Self-organizing Systems, Martin-Luther-Universität Halle-Wittenberg, Halle (Saale), Saxony-Anhalt, Germany
[b] Interdisciplinary Research Center HALOmem at the Martin-Luther-Universität Halle-Wittenberg, Germany
[c] Institute of Biochemistry, Physical Biotechnology, Martin-Luther-Universität Halle-Wittenberg, Halle (Saale), Germany
[d] Biocenter, Martin-Luther-Universität Halle-Wittenberg, Halle (Saale), Germany
[e] Department of Molecular and Cellular Biology, University of Guelph, Guelph, Ontario, Canada

ARTICLE INFO

Keywords:
Intrinsically disordered protein (IDP)
Transmission electron microscopy
Electron paramagnetic resonance
Dynamic light scattering

ABSTRACT

Myelin basic protein (MBP) is an intrinsically disordered protein and in the central nervous system (CNS) mainly responsible for connecting the cytoplasmic surfaces of the multilamellar, compact myelin. Increased post-translational modification of MBP is linked to both, the natural development (from adolescent to adult brains) of myelin, and features of multiple sclerosis. Here, we study how a combination of this intrinsically disordered myelin protein with varying the natural cholesterol content may alter the characteristics of myelin-like membranes and interactions between these membranes. Large unilamellar vesicles (LUVs) with a composition mimicking the cytoplasmic leaflet of myelin were chosen as the model system, in which different parameters contributing to the interactions between the lipid membrane and MBP were investigated. While we use cryo-transmission electron microscopy (TEM) for imaging, dynamic light scattering (DLS) and electrophoretic measurements through continuously-monitored phase-analysis light scattering (cmPALS) were used for a more global overview of particle size and charge, and electron paramagnetic resonance (EPR) spectroscopy was utilized for local behavior of lipids in the vesicles' membranes in aqueous solution. The cholesterol content was varied from 0—60 % in these LUVs and measurements were performed in the presence and absence of MBP. We find that the composition of the lipid layers is relevant to the interaction with MBP. Not only the size, the shape and the aggregation behavior of the vesicles depend on the cholesterol content, but also within each membrane, cholesterol's freedom of movement, its environmental polarity and its distribution were found to depend on the content using the EPR-active spin-labeled cholesterol (CSOSL). In addition, DLS and EPR measurements probing the transition temperatures of the lipid phases allow a correlation of specific behavior with the human body temperature of 37 °C. Overall, our results aid in understanding the importance of the native cholesterol content in the healthy myelin membrane, which serves as the basis for stable and optimum protein-bilayer interactions. Although studied in this specific myelin-like system, from a more general and materials science-oriented point of view, we could establish how membrane and vesicle properties depend on cholesterol and/or MBP content, which might be useful generally when specific membrane and vesicle characteristics are sought for.

1. Introduction

Multiple sclerosis (MS) is a neurodegenerative disease of the central nervous system that is believed to be caused by an autoimmune attack [1,2]. Demyelination, i.e. the gradual degradation of the myelin sheath, can be viewed as the hallmark of the disease, which proceeds by loss of the electric isolation of the axon. This leads to a defective signal transduction that finally results in the loss of motoric and sensory skills. Many

* Corresponding author at: Institute of Chemistry, Physical Chemistry – Complex Self-organizing Systems, Martin-Luther-Universität Halle-Wittenberg, Halle (Saale), Saxony-Anhalt, Germany.
E-mail address: dariush.hinderberger@chemie.uni-halle.de (D. Hinderberger).

https://doi.org/10.1016/j.bbamem.2023.184179
Received 8 December 2022; Received in revised form 23 April 2023; Accepted 20 May 2023
Available online 25 May 2023

myelin proteins form antigens that are linked to MS and myelin basic protein (MBP) is one of the most abundant ones in the CNS. The demyelination is, regarding MBP, dependent on the MBP concentration [3], the number of post-translationally modified protein variants, the lipid composition and the ion content [4,5].

MBP is an intrinsically disordered protein (IDP) [6,7] and the 18.5 kDa splice isoform is predominant in the adult human brain. This variant shows multifunctionality [8,9], structural polymorphism, a high net charge (+19 at pH 7), and charge adaptation by post-translational modifications (PTMs) through especially citrullination and phosphorylation altogether leading to a variety of physical-chemical properties. [1,10] Here, the focus is on the ability of MBP to stack multiple myelin membranes together to form a compact myelin sheath. The animal model of MS, experimental autoimmune encephalomyelitis (EAE), mimics the MS disease in later stages. [4,11] In this model the amount of charge-reduced variants is higher and also the lipid composition changes (increasing phosphatidylserine (PS), phosphatidylethanolamine (PE) and cholesterol, decreasing phosphatidylcholine PC, sphingomyelin (SM) and phosphatidylinositol (PI) amount). [11,12] One consequence is that the ability to stack membranes tightly is reduced. The three amphipathic α-helices that form in vicinity of lipid bilayers are the main interaction sites of MBP with a membrane. [13,14] The positive net charges of MBP are one major driving force that lead to protein folding and partial insertion into the bilayer, as they interact electrostatically with the negatively charged lipid bilayers. [15,16]

In the case of MBP, which is a peripheral membrane protein, large unilamellar vesicles (LUVs) can be utilized as simplified model system for in vitro studies. One may have a more differentiated view on the model membrane studied in comparison to multilamellar vesicles (MLVs). MLVs may represent, next to nanodiscs [17,18], the model that was considered closest to the natural structure of the myelin sheath and therefore were mainly used early to investigate membrane-protein interactions. Emphasis in previous studies was placed, among other aspects, on the impact of changes in lipid composition. To test the influence of the lipid composition on the MBP-lipid interaction the lipid contents were varied: changing one selected lipid such as phosphatidylcholine (PC) [19], varying contents of two or three [19,20] main lipids of the cytoplasmic myelin membrane, or testing the full extract composition [5,21,22]. In a previous study, we have shown that the cholesterol content in lipid monolayers at the air-water interface is important for the interaction with MBP even though the cholesterol and protein seem not to interact directly. [23] Monolayers with a 44 % cholesterol content (natural amount in healthy adults) appear to form more thermodynamically stable monolayers and show unique features in comparison to monolayers with lower or higher cholesterol content. Adding MBP to monolayers with the natural adult cholesterol content has the biggest improvement in stability at surface pressures of 35 mN m^{-1}. Even though we have shown that the monolayer model is a robust mimic for the whole myelin in some aspects, here we extend our work to LUVs as a bilayer model. Lipids may act differently when included in a bilayer as opposed to a monolayer system because of, e.g., the appearance of curvature of the outer and inner side, freedom of motion, and membrane specific mechanisms such as flip-flops. LUVs as model membranes should have a minor impact on the lipid-protein interactions (as MBP is an peripheral membrane protein) and provide a homogeneous lipid environment regarding their size and shape. Besides their use as membrane model systems, they are of interest also technologically, e.g. in formulation/delivery of all kinds of (small molecules/nucleic acid etc.) drugs. Hence, understanding the impact of individual membrane components of a complex mixture on overall LUV shape, properties, and local lipid effects is of great interest, too. Here, we use a lipid composition similar to that of the cytoplasmic leaflet of myelin, which consists of phosphatidylcholine (PC), phosphatidylserine (PS), phosphatidylethanolamine (PE), sphingomyelin (SM), and phosphatidylinositol (PI) at molar ratios of 11:13:27:3:2 and variable ratios of cholesterol, which natively makes up 44 %. [24] MBP specifically interacts with the cytoplasmic side of myelin and in our previous studies was found to be located mainly at the border of cholesterol/SM-rich phases and phospholipid-rich phases. [23,25,26] Hence, besides aiming at understanding of how MBP interaction in curved lipid-bilayer membranes depends on cholesterol content, we chose varying cholesterol and MBP content to tune the LUV properties inside the bilayer membrane and globally.

Cholesterol is amphiphilic but has a significantly different structure compared to other membrane lipids. Whereas phospholipids consist of a hydrophilic headgroup and two hydrophobic acyl chains, cholesterol has a short isooctyl chain, a rigid planar steroid ring system and a small polar hydroxyl group. Cholesterol positioning in the lipid layers is such that the hydroxyl group is located towards the headgroups of the phospholipids and the plate-like ring system is positioned parallel to the phospholipid acyl chains reaching a depth of neighboring phospholipid C9-C10 carbon atoms. [27–29] The short acyl chain points to the membrane center. Cholesterol is known to interrupt headgroup-headgroup interactions [30] and forms regions that are enriched in cholesterol and sphingolipids [31,32]. These regions are highly ordered and rigid, leading to a reduced fluidity of the whole membrane.

In the following, we present work on myelin-like LUVs with varying cholesterol contents (10 %, 20 %, 30 %, 40 %, 44 % (natural amount), 50 %, and 60 % cholesterol) using different techniques of characterization on varying length and time-scales. All experiments were performed with and without MBP to investigate the influence of the cholesterol content on the interaction of MBP with the lipid bilayer. Dynamic light scattering (DLS), continuously monitored phase analysis light scattering (cmPALS) and cryo-transmission electron microscopy (cryo-TEM) allowed insights on the more global behavior of the LUVs, whereas EPR spectroscopy of a spin-labeled cholesterol derivative (CSOSL, see [30]) enabled studying membrane properties such as hydrophobicity, fluidity, and motion freedom directly at the cholesterol position.

2. Materials and methods

2.1. Materials

Bovine myelin basic protein 18.5 kDa (MBP) was purchased from Merck KGaA (Darmstadt, Germany). Buffer solution of *N*-(2-hydroxyethyl)piperazine-*N*′-ethanesulfonic acid (HEPES) and sodium chloride (both from Merck KGaA) was prepared with ultrapure water from a Milli-Q Advantage A10 (Millipore S.A.S., Molsheim Cédex, France) with a conductivity lower than 0.055 μS cm^{-1}, and adjusted with sodium hydroxide (Fisher Scientific, Leicestershire, U.K.) to pH 7.4. MBP was dissolved in HEPES-NaCl-buffer (20 mM HEPES, 10 mM NaCl, pH 7.4) resulting in a stock concentration of 100 or 300 μM and stored at 4 °C. The lipids porcine brain L-α-phosphatidylcholine (PC), porcine brain L-α-phosphatidylserine (PS), porcine brain L-α-phosphatidylethanolamine (PE), porcine brain sphingomyelin (SM), bovine liver L-α-phosphatidylinositol (PI) and cholesterol (ovine wool) were purchased from Avanti Polar Lipids (Alabaster, USA). HPLC grade chloroform was purchased from Carl Roth GmbH & Co. KG (Karlsruhe, Germany). Glycerol (87 wt% in water, ACROS Organics, Belgium) and all other substances mentioned above were used without further purification. The carboxy-TEMPO spin labeled cholesterol (CSOSL) was synthesized as in T. Hauenschild et al. [33].

2.2. LUV preparation

Large unilamellar vesicles (LUVs) were prepared by dissolving all lipids in chloroform (stored at —30 °C) and mixing them together in a glass vial in the composition similar to that of the cytoplasmic leaflet of myelin (porcine brain L-α-phosphatidylcholine (PC), porcine brain L-α-phosphatidylserine (PS), porcine brain L-α-phosphatidylethanolamine (PE), porcine brain sphingomyelin (SM), bovine liver L-

α-phosphatidylinositol (PI) with a molar ratio of 11:13:27:3:2) [23,24,34]. The cholesterol content was varied to following final molar percentages: 0 %, 10 %, 20 %, 30 %, 35 %, 40 %, 44 %, 50 %, 60 % with the remaining lipids being always adjusted to the same molar ratio. Secondly, the chloroform was evaporated under a nitrogen stream, resulting in a dry lipid film. The lipid film was then frozen at −30 °C and thawed at room temperature. To rehydrate the lipid film, a defined volume of buffer (20 mM HEPES, 10 mM NaCl, pH 7.4) was added onto the dry lipid film (volume depends on the measuring method and thereby concentration needed). The glass vial with lipid film and buffer was then placed in a water bath (45 °C) with sonication for 10 min twice. Intermittently and after the swelling procedure, the vesicle suspension was vortexed to loosen the vesicles from the bottom of the flask and to downsize them. To achieve a homogeneous size of 100 nm diameter and reduce multilamellarity, the vesicle suspension was extruded (Avanti Lipid extruder, equipped with a polycarbonate membrane, 100 nm pore size) 31 times at 45 °C, and stored over-night at 4 °C. All vesicle suspensions were used on the next day and up to 3 days afterwards.

2.3. Cryo-transmission electron microscopy (cryo-TEM)

Cryo-TEM grids were prepared by applying aqueous samples to glow-discharged copper grids covered with a holy carbon film (C-flat™, Protochips Inc., Raleigh, NC, USA) and then blotting with a filter paper. Vitrification was achieved using a Leica Grid Plunger GP1 (Wetzlar, Germany) with 95 % humidity and a blotting time of 15 s. Imaging was performed with a LIBRA 120 plus (Carl Zeiss Microscopy, Jena, Germany; 120 kV) transmission electron microscope equipped with a Gatan 626 cryotransfer system. Using the iTEM software (Olympus SIS, Münster, Germany) micrographs were taken with a dual-speed on axis SSCCD camera (BM-2k-120; TRS, Moorenweis, Germany). A lipid concentration of 1—1.5 mg mL^{-1} and a lipid to MBP molar ratio of 567:1 [35] was applied. The lipid-protein mixtures were incubated for 15 min at room temperature prior to grid preparation.

2.4. Dynamic light scattering

Dynamic light scattering measurements were performed with an Litesizer 500 device (Anton Paar GmbH, Graz, Austria). The aqueous suspensions of LUVs (1.1 mM) with different cholesterol content (0 %, 10 %, 20 %, 30 %, 35 %, 40 %, 44 %, 50 %, 60 %) in HEPES-NaCl buffer (20 mM HEPES, 10 mM NaCl, pH 7.4) were poured into a quartz cell (Hellma Analytics, Müllheim, Germany). All samples were measured in a temperature interval of 0—60 °C, recorded at a side-scattering detection angle of 90° relative to the incident monochromatic light (He—Ne laser $\lambda = 658$ nm). At 20 °C, it was also recorded at a back-scattering detection angle of 175°. At each temperature, 6 runs of 30 s with an equilibration time of 9 min and an automatic focus were performed. Software input for analysis was a general analysis model, the Cumulant model, and water as a solvent (for refractive index $n_{H2O} = 1.33$ and viscosity $\eta = 1.0019$ mPa·s at 20 °C). The hydrodynamic diameters were calculated using the Kalliope software provided by Anton Paar and additionally the autocorrelation functions were analyzed using the ALV-5000/E/EPP software. Further description of calculation can be found in the SI. The incubation time for MBP with the LUVs was 15 min before measuring with the same setup as for the LUV suspension. The molar ratio of lipids to protein was 567:1, as described above.

2.5. Continuously monitored phase-analysis light scattering (cmPALS)

Sample preparation for cmPALS measurements was the same as for DLS measurements. The Litesizer 500 device was equipped with an Univette cuvette (Anton Paar GmbH, Graz, Austria) that prevents electric field gradients at the measurement position. By using the LASER Doppler velocimetry (LDV) technique in an electrophoretic light scattering (ELS) setup, the zeta potentials were obtained by measuring the electrophoretic mobility at 20 °C. A constant voltage of 11 V was applied. The ionic strength for the HEPES-NaCl buffer at pH 7.4 was $I = 0.018$ M. The Debye factor was calculated with the hydrodynamic diameter from DLS measurements. Data analysis was performed with the continuously monitored phase-analysis light scattering technology (cmPALS), provided in the software package Kalliope 10.02.2002. Further information in SI.

2.6. Electron paramagnetic resonance (EPR) spectroscopy

2.6.1. Continuous wave (CW) EPR

For CW EPR experiments, stock solutions of 1.1 mM LUVs containing 0 %, 10 %, 20 %, 30 %, 35 %, 40 %, 44 %, 50 %, and 60 % cholesterol were prepared in HEPES-NaCl buffer. In all samples, carboxy TEMPO spin-labeled cholesterol, CSOSL, amounted to 4.4 % of all lipids (50 μM). The bovine MBP stock solution had a concentration of 100 μM. For experiments with protein an incubation period of 15 min was chosen and a lipid to MBP molar ratio of 567:1 [35] was used. 15 μL of the sample volume was placed into a quartz capillary (BLAUBRAND IntraMARK) with about 1 mm outer diameter. An X-band Miniscope benchtop spectrometer MS400 (Magnettech GmbH, now part of Bruker Biospin, Ettlingen, Germany) was used at microwave frequencies of about 9.4 GHz, equipped with a frequency counter (RACAL DANA, model 2101) and a temperature controller H03 (Magnettech GmbH, Berlin, Germany). For all samples a temperature series was performed in the range of −10 °C to 80 °C using modulation amplitudes of 0.2—0.1 mT, sweep widths of 15 mT, 8—16 scans at 60s per scan, and microwave powers of 5—10 dB. A detailed evaluation of data from EPR spectroscopy can be found in the SI.

2.6.2. Double electron-electron resonance (DEER)

All 4-pulse DEER experiments were performed at X-band frequencies of 9.3—9.6 GHz at 50 K. Experiments were performed with a BRUKER Elexsys E580 spectrometer equipped with a BRUKER Flexline splitring resonator ER4118X-MS3, and over-coupling the resonator to $Q < 200$. Cooling was achieved by a closed cycle cryostat (ARS AF204, customized). The maximum of each field-swept electron-spin-echo (ESE)-detected spectrum was used as the pump frequency υ_{pump}. The observer frequency υ_{obs} was set to $\upsilon_{pump} + \Delta\upsilon$, with $\Delta\upsilon$ being in the range of 70 MHz and therefore coinciding with the low field local maximum of the nitroxide ESE spectrum. The pulse sequence used was: $\pi/2(\upsilon_{obs})$-τ_1-$\pi(\upsilon_{obs})$-t'-$\pi(\upsilon_{pump})$-(τ_1 + τ_2-t')-$\pi(\upsilon_{obs})$-τ_2-echo with $\tau_2 = 1.5$ μs. A detailed evaluation of data from EPR Spectroscopy can be found in the SI.

3. Results and discussion

3.1. Cryo-transmission electron microscopy (Cryo-TEM)

LUVs with 20 %, 44 %, and 60 % cholesterol content were prepared (keeping the molar ratio of the other lipids constant; PC/PS/PE/SM/PI 11:13:27:3:2) and studied with and without addition of MBP (lipid to protein ratio 567:1 [35]) via cryo-TEM. The cholesterol levels of 20 % (example from the low percentage range) and 60 % (maximum value) were selected to give an overview of the effect of increasing and decreasing the natural content of 44 %. In several studies, the “gluing” effect of MBP on a model membrane, i.e. its capability of adjoining two opposing membrane leaflets, has already been demonstrated via TEM [4,5,20,21].

Fig. 1 (A—C) shows the cryo-TEM images of LUVs without MBP. Regardless of the cholesterol content, the LUVs are clearly separated from each other and have a predominantly round shape. This finding is correlated with the DLS data (discussed later on). In addition to isolated bi- or multilamellar vesicles, the cryo-TEM images depict a large number of unilamellar vesicles.

Shaharabani et al. [4,5] have shown using SAXS and cryo-TEM that

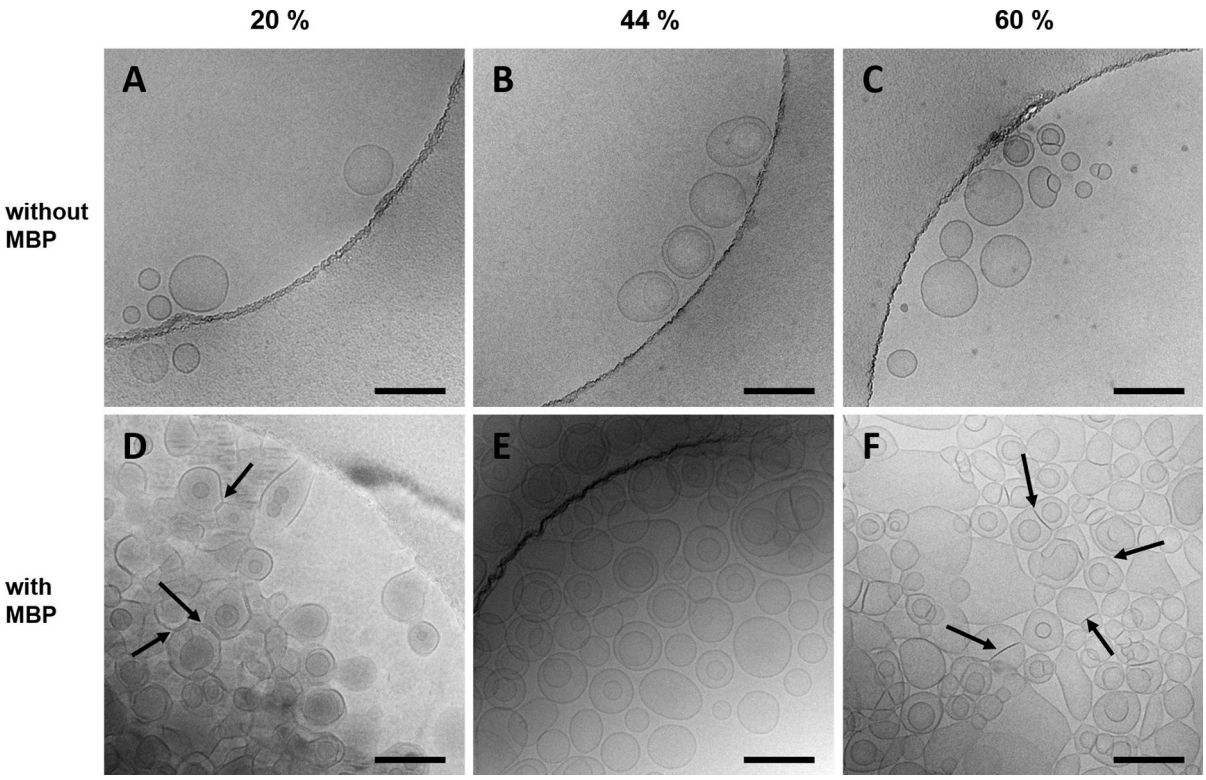

Fig. 1. Cryo-TEM images of vesicles with 20 % (A, D), 44 % (B, E), and 60 % (C, F) cholesterol content with (D—F) and without (A—C) MBP in a HEPES-NaCl-buffer. The black arrows mark areas with special features: a) punctate contacting, b) areas with higher density. The scale bar represents 200 nm.

in MLVs with a lipid composition similar to that of people with and without MS disease there are differences in lipid phases even without MBP. In MLVs with a lipid composition of MS patients (here comparable to 60 % cholesterol content) a strong change in the curvature of the membrane could be determined. They observed that in the inverted hexagonal phase, which coexists with the lamellar phase, the membrane undulates with great local curvature [4,5]. Such a curvature cannot be observed in this study. This could be due to the unilamellar system and the slightly different lipid composition (additional PI) used. In addition, a different buffer system (MOPS, here HEPES) and much higher salt concentrations (150 mM, here 10 mM) were used. The difference in the buffer system may be seen as negligible, but previous studies have shown an influence of the salt concentration on the organizational behavior of the lipids [5].

The images of vesicles with MBP depict a clear difference than those without MBP (Fig. 1D—F, see details in Fig. S4). The vesicles, in general, stick together and form bigger aggregates independent of the cholesterol content. However, upon closer inspection differences appear in the shape and the distances between the membranes, which seem to depend on the cholesterol content. After the addition of MBP to LUVs with 20 % cholesterol content (Fig. 1D), a strong deformation of the round shape can be observed, apparently leading to maximized contacting areas between membranes of opposing vesicles (see black arrows). It seems that between the vesicles no free space (volume) is detectable. Adding MBP may even pull two membranes closer together, probably minimizing the water content in between. This deformation may possibly be traced back to the lower content of cholesterol in the bilayer. Cholesterol in general is not necessary for interaction with MBP, however the decreased fluidity of the membrane induced by cholesterol is of great importance for the structured layer formation in myelin [3,36]. A higher cholesterol content results in a more rigid membrane because more cholesterol-enriched areas are present that are defined by a higher local order and therefore a loss of mobility in comparison to the surrounding phospholipid-enriched areas. LUVs with a low(er) cholesterol content may thus be flexible enough to deform. Also, the amount of negatively charged lipids is higher (overall), giving MBP more available interaction sites.

Vesicles containing 60 % cholesterol (Fig. 1F) differ slightly from vesicles with 20 % cholesterol. In both samples, opposing vesicles actually have areas of direct membrane contact. The 60 % cholesterol sample show contacts that partially seem to be more punctate (right black arrow Fig. 1F). The seemingly lower contact surface could be due to the reduced amount of negatively charged lipids: MBP-based membrane contacts can only take place where MBP can bind and this surface is reduced. In addition, regions with a higher electron density are visible as darker shades in the images (black arrows). These contacts form an almost linear arrangement of membranes at bordering vesicles. The image even suggests that one single bilayer is observed: two opposing bilayers are not visible. On the one hand, these suspected density differences could be caused by different thicknesses of the vitreous ice layers and contrast adjustments. On the other hand, due to the fact that almost no curvature is observed in the regions with higher density and the rest of the vesicle shows normal curvature, it is suspected that those contact regions are high in cholesterol content. The excess cholesterol accumulates and therefore builds a very rigid bilayer that has minor flexibility. This stiff bilayer could be the cholesterol bilayer domains (CBD) described by Subczynski et al. [29], a pure transmembrane cholesterol bilayer without any phospholipids. These form at high cholesterol contents above 50 % (in single lipid samples). Raguz et al. [37] observed that with mixing ratios higher than 2.5 of cholesterol: phospholipids, next to the coexistence of both components, the CBDs appear as a second domain. Here, we don't exceed the ratio of 1.5, but taking into account that we use a much more complex lipid composition, the formation of CBDs could be induced at lower ratios.

Indeed, a higher cholesterol content is found in the membrane model of the induced inflammatory disease experimental autoimmune encephalomyelitis (EAE). [11,38] This animal model of MS is widely used and shows many similarities to MS in humans in its later stages. It

has been shown that multilayers of the EAE composition do not form a homogenous layering [4] and lamellar and inverted hexagonal phases coexist [5] (not observed here). The diseased membrane (represented here with a cholesterol content of 60 %) would not form an evenly compact myelin sheath due to the differences in density and thus also in thickness. Shaharabani et al. [4]. postulated from a wave-like deformation of the membrane (in vitro as well as in vivo) the spontaneous induction of pores. These pores make the membrane vulnerable to attacks by the immune system [5]. By having a myelin sheath that is not constant in layer spacing, compaction and density around the axon, the signal transduction could malfunction and result in the hallmark consequences of MS, demyelination with ensuing physiological consequences such as loss of motor and sensory skills.

Finally, LUVs containing the natural cholesterol content of 44 % were studied with and without MBP (Fig. 1B, E). With MBP bound, the LUVs are circular, similar to the LUVs without MBP. There is no direct contact area and no strong deformation of the membranes as it was found with 20 % and 60 % cholesterol content. As shown in our previous monolayer study [23], the cholesterol content of 44 % presents a delicately balanced state compared to the other lipid mixtures. The natural composition combines a (presumably) thermodynamic stability with an optimum protein interaction and that results, here, on a more macroscopic scale, in a more orderly adhesion of the vesicles. The regularity in shape and distance is a good prerequisite for a homogeneous layering of the myelin sheath as it is needed in a healthy brain.

One may thus conclude from the cryo-TEM images that with too little or too much cholesterol, the nature of the vesicles changes so dramatically that homogeneous layering and ordered adhesion cannot be achieved. With low cholesterol content (20 %) the vesicles are strongly deformed and seem to maximize the contact area. This is related to a lower rigidity of the bilayer, which is mainly induced by cholesterol and the relative higher amount of negatively charged lipids that are the main interacting partners for MBP. At high cholesterol contents (60 %), a different type of deformation of the bilayer is observed. The contacting area is not overall maximized and locally areas of higher density occur. The selective behavior could result from the higher rigidity of the vesicles and the reduced amounts of PS and PI. This case can be viewed as an oversaturation with cholesterol, so that large rafts could form that show a higher density because of a higher packing order. This however, needs to be investigated in more detail. Only the 44 % cholesterol content assures the homogeneous membrane order of the vesicles. One may infer that this behavior may add to provide a basis for a

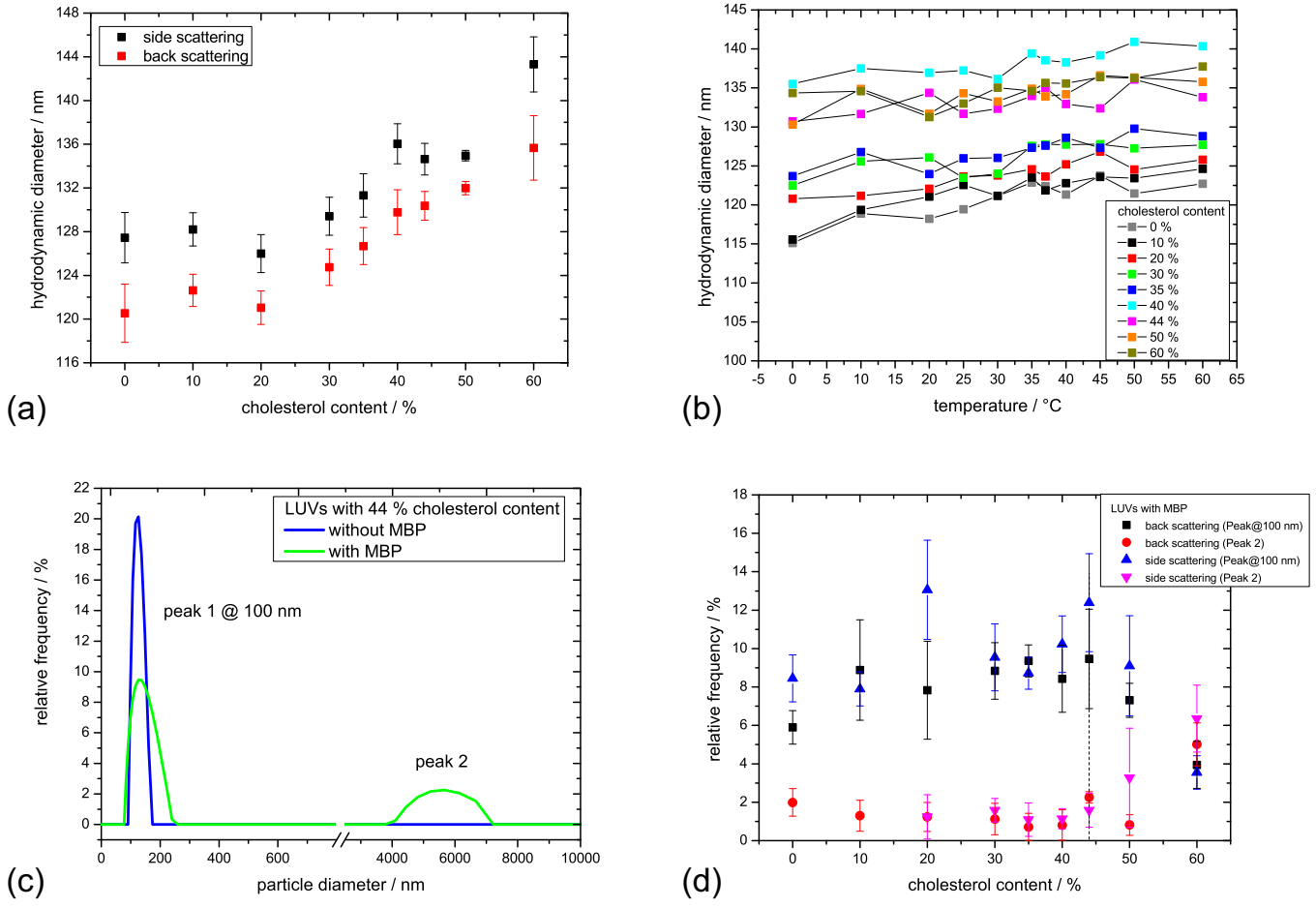

Fig. 2. (a) Hydrodynamic diameter of LUVs in dependence of cholesterol content obtained by dynamic light scattering with scattering angles of 90° (black) and 175° (red) at 20 °C (intensity-weighted). Error bars represent the standard error of mean of three measurements. (b) Temperature series of hydrodynamic diameter of LUVs with different cholesterol content obtained by dynamic light scattering in a HEPES-NaCl buffer with a scattering angle of 90° (intensity-weighted) and a temperature interval of 0—60 °C. (c) Dynamic light scattering, intensity-weighted distributions of hydrodynamic particle diameter of LUVs containing 44 % cholesterol with and without MBP (2 μM) (measured at 20 °C in a HEPES-NaCl buffer with scattering angle of 175°). Bimodal distribution of LUVs with MBP consisting of a peak 1 at 100 nm (individual LUVs) and a further peak 2 (LUV-MBP aggregates) at much larger diameters. (d) Dynamic light scattering intensity-weighted peak maxima of hydrodynamic particle diameter of cholesterol containing LUVs with MBP (2 μM) measured at 20 °C in a HEPES-NaCl buffer with scattering angle of 175° (back-scattering) and 90° (side-scattering). Peak@100 nm and peak 2 relate to the peaks of the bimodal particle size distribution defined in panel c. The dashed line at 44 % cholesterol content visualizes the transition point of the aggregation behavior. Error bars represent the standard error of the mean of three measurements. (For interpretation of the references to colour in this figure legend, the reader is referred to the web version of this article.)

homogeneous layering of the myelin sheath. From a more technological point of view, the native lipid composition with 44 % cholesterol shows a remarkable rigidity in its membranes, even when a known adhering protein like MBP is added. Given the strong deformations that, on the other hand, are possible at 20 % and 60 % cholesterol, such an intermediate (but high overall cholesterol) content might be seen as a tuning parameter for rigidity, interaction surface and overall deformation.

3.2. Dynamic light scattering (DLS)

Dynamic light scattering experiments were carried out to characterize the size and shape of the vesicles and their aggregation behavior in solution. Here, a buffer of HEPES and sodium chloride was used with an ionic strength of 18 mM. To characterize the size and particle shape, measurements at room temperature (20 °C) were performed for two different scattering angles: 90° (side-scattering) and 175° (back-scattering). For the LUVs without MBP, narrow monomodal size distributions (polydispersity index (PDI) <12 %, transmission >80 %, see SI S5) were obtained at averaged hydrodynamic particle diameters of 126.0 nm ± 2.5 nm for both angles and for all three different cholesterol mixtures (Fig. 2a). This shows that the extruded particles are spherical (negligible size difference of LUVs at both angles) independent of the cholesterol content. This may be expected, as already seen in the cryo-TEM data. A small rise in size is noticeable from 30 % cholesterol content upwards, at both scattering angles. Adding more cholesterol leads to a larger separation of the headgroups of the phospholipids. [39,40] This could lead to a higher content of incorporated water in LUV bilayers with higher cholesterol content and a subsequent swelling of the LUVs. This is caused by induced packing defects in the chain region that create free space which can be accessed by surrounding water molecules. Hence, the lipids need more space and the vesicle diameter expands, which is also in agreement with the broader distribution peaks at higher cholesterol contents (see SI). Swelling because of osmolality differences seems not very likely as the used buffer and buffer strength were identical.

Number-weighted analysis of the DLS data confirms that all LUV mixtures contain mainly particles of the size of the hydrodynamic diameter (SI S5b). Additionally, temperature series of each LUV mixture with different cholesterol content were performed in a temperature range from 0—60 °C at side-scattering. Fig. 2b shows the hydrodynamic diameter as a function of the temperature. In general, and independent of the cholesterol content, there is a small rise of diameter with higher temperature of approximately 6 nm. This could be caused by the lipids undergoing the transformation from a crystalline-like phase to a gel-like phase and then into a fluid phase at high temperatures. These phase changes correlate with a change in conformation from *all trans* to mainly *trans* and then to the *gauche* conformation in which the lipids occupy larger volumes/areas due to the change in the lipid packing parameter (the ratio between the headgroup size and the projected hydrocarbon chain area). [41–43]

Temperature also has an effect on the intermolecular forces between the water molecules. This, in turn, changes their effective hydrophobic interactions and thus the order of the water layer in the vicinity of the lipid bilayer [44]. It can be observed that there are slight differences in size in dependence of the cholesterol content, as already observed in Fig. 2a. LUVs containing 40 %, 44 %, 50 % and 60 % cholesterol have higher diameters of ca. 130—140 nm, and those at 0 %, 10 %, 20 % 30 %, and 35 % are at ca. 115—127 nm. When inspecting the intensity-weighted, temperature-dependent DLS particle diameter peak maxima of cholesterol containing LUVs (Fig. S5c) one finds that all LUVs show high intensities between 8—20 % and have monomodal distributions. The smallest statistical spread occurs at temperatures of 35 °C and 37 °C. LUVs with different cholesterol content are in general spherical and stable at varying temperatures, but show minimal changes in the hydrodynamic diameter in dependence of the cholesterol content.

DLS measurements with MBP are not reproducible in a straightforward way. Peaks indicating sizes in the micrometer range appear, whose maxima and shape may only be taken as rough trends and individual measurement series are shown below as examples. The reproducibility of the peaks is difficult as MBP forms aggregates of a broad size range. The broadly size-ranged aggregates lead to discontinuities in the recorded count rates. These discontinuities are transferred to the calculated correlation functions and particle size distributions, which makes quantification particularly difficult.

Performing the DLS measurements of the described LUVs with MBP, the results show that in addition to the peak at 126 nm a second peak arises at particle diameters >200 nm, giving an overall bimodal distribution (PDI < 40 %, transmission <60 %, Fig. 2c depicts the 44 % cholesterol sample as an example; see the SI for all distributions). The peak at higher sizes is further evidence that MBP "glues" the vesicles together and forms larger aggregates that can, e.g., be seen in the cryo-TEM images. Also, the transmission changes from >80 % in pure LUV samples to lower percentages of <60 % for LUV + MBP samples, which is a clear sign for formation of differently sized particles. The persistence of the peak at 126 nm shows that not all vesicles adhere to neighboring vesicles by MBP. In the number-weighted analysis one finds vesicles (126 nm), protein-vesicle aggregates (>200 nm), and single MBP molecules/dimers (10 nm) (see number-weighted distributions in SI S6c). Measurements of pure bMBP in buffer show that MBP molecules occur in the range of 3—10 nm and numerically rarely form large aggregates (see S6d). Also, the numerical ratio of large aggregates to LUVs is very small, i.e., just a few bigger aggregates are formed and the main population of particles still consists of single LUVs. In the intensity-weighted measurements at 20 °C (back- and side-scattering) of LUVs with MBP (Fig. 2d), it is clear that the aggregation behavior changes above a cholesterol content of 44 %. The intensity relation from a high intensity peak 1 to a low intensity peak 2 is changing to a lower intensity peak 1 and a higher intensity peak 2, in both side and back-scattering (see Fig. 2c for peak definition). This trend can be observed over the entire temperature range tested (S6e). As in the previous samples without MBP, a temperature dependence can be deduced from the autocorrelation functions of the samples with MBP. As the temperature rises, the correlation function is shifted to shorter times (see S6b). This observation may likely result from the dominance of the reduction in viscosity when the temperature increases. The temperature-induced swelling of the vesicles is most likely not suppressed by MBP, or rather the proportion of non-aggregated LUVs is too high to be able to make a specific statement regarding the direct MBP effects.

Dynamic light scattering experiments have shown that vesicles without MBP are in general spherical and stable at all measured temperatures for all cholesterol contents studied. Interestingly, the hydrodynamic diameter shows minimal changes depending on the cholesterol content. DLS experiments of LUVs with MBP result in a highly increased particle size, reflecting MBP-induced aggregation behavior, which is in line with the findings in the cryo-TEM images that MBP leads to inter-particle aggregates. One may retrospectively assume that the solution-based findings in DLS and the conclusions drawn from the cryo-TEM images are directly complementary. The protein vesicle interactions of LUVs containing 0—20 % cholesterol are temperature dependent. The aggregation behavior changes above 44 % cholesterol content in the LUVs and marks 44 % cholesterol again as the prominent lipid composition. The temperature range of 35—40 °C (human body temperature) in both experimental series seems to be important as a point of change.

3.3. Zeta potential

The zeta potentials were obtained by measuring the electrophoretic mobility at 20 °C. To this end, LASER Doppler velocimetry (LDV) in an electrophoretic light scattering (ELS) setup (see further information in SI) was used. Measurements of the zeta potential ζ can give insight to the membrane potential at the position of the slipping plane of a solvated particle [45,46]. The membrane potential is influenced by the

adsorption or insertion of charged molecules as MBP. It is dependent on pH, ionic strength, and concentration of the sample. [47]

The LUVs were measured at a physiological pH of 7.4, a high ionic strength of 18 mM, a temperature of 20 °C and a concentration of 1.1 mM and show a transmission of over 80 % for the pure vesicle dispersion (with each lipid mixture). With this lipid composition including negatively charged lipids PS and PI, the vesicles should be negatively charged at the surface. Indeed, an averaged mean zeta potential value of —53.1 mV ± 7.8 mV for the LUVs with different cholesterol content is found (Fig. 3). All vesicles show monomodal distributions of ζ values (see SI S7). As can be seen in Fig. 3, the zeta potential of the vesicles is independent of the cholesterol content. In cell membranes, the composition of the inner and outer monolayers is asymmetrical, as the curvature of the membrane and possible stress must be balanced. The observed independence on the cholesterol content may possibly be achieved by an equal ratio of available space (not occupied by cholesterol) to number of negatively charged lipids. Resulting in the same amount of lipids with negative charge on a defined membrane area.

Adding MBP to the vesicles results in a rise of the zeta potential on average to —27.9 mV ± 4.9 mV (Fig. 3). This is due to the positively charged MBP neutralizing the negative charges of the phospholipids. From previous studies on lipid-MBP interactions, it is known that the first step after electrostatic attraction is charge neutralization by MBP. Thus, it was expected that the addition of MBP lowered the negative surface charge of the lipids as the charge is partially compensated by MBP molecules. [3,9] Although the absolute amount of negatively charged lipids in the mixtures changes, decreasing with higher cholesterol content, the zeta potential does not change depending on the cholesterol content. This could mean that the ratio of negative lipids to positive protein is so high that MBP is saturated even in the vesicles with 60 % cholesterol content and the excess negative charges dominate the overall charge. From the DLS data it is known that not all LUVs get adhered together by MBP, there are individual LUVs left because the peak at 126 nm is still present. Therefore, the value of zeta potential for samples with protein is an average of the larger aggregates adhered together by MBP and individual LUVs. The surface potential of a single MBP-vesicle aggregate could be at more positive values considering that pure MBP in buffer has a zeta potential of 8.9 mV ± 0.5 mV (S7B). In the TEM images in Fig. 1, areas with a higher density could be identified for 60 % cholesterol content, always located between two vesicles. Therefore, they cannot be detected by ELS. The assumption suggested above that these areas represent increased cholesterol levels would support the negligible influence of cholesterol on zeta potential values. In the overall balance of the shear plane detectable by ELS, these areas would therefore be missing, i.e. the relative contribution to the accessible surface would be reduced and hence a higher negative potential than expected from an average value is found. Furthermore, the zeta potential seems not to be correlated with the surface charge of the vesicles but just the slipping plane that is influenced by the buffer and its ions. The zeta potential measurements with MBP can only be analyzed on a general level as the particle size is very large, and therefore the transmission at a lower acceptance level for the implemented analysis model. In order to obtain details about the actual lipid surface, measurement methods were carried out, which primarily examine the local area around the surface of the lipid bilayer.

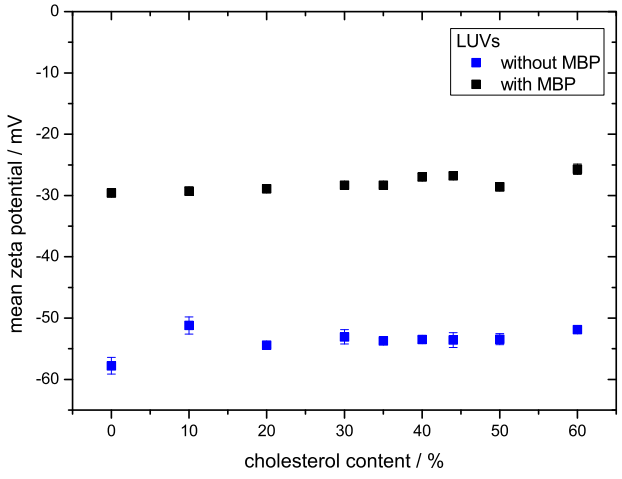

Fig. 3. Continuously-monitored phase-analysis light scattering (cm-PALS): mean zeta potential of cholesterol containing LUVs with and without MBP (2 μM) in a HEPES-NaCl buffer (measured at 20 °C with maximum 40 V, 200×). Lipid to protein ratio is 567:1, respectively. Error bars represent the standard error of the mean of three measurements.

3.4. EPR spectroscopy

We have used an EPR-active spin label that is introduced into the cholesterol to observe the influence of the MBP binding on the lipids using EPR-spectroscopic techniques. The hydroxyl group of cholesterol is used to this end and is esterified with 4-carboxy-TEMPO to form a cholesterol spin label (CSOSL) [33] (Fig. 4). The structural alteration in CSOSL compared to CSO seems moderate when considering that still a strongly hydrophobic steroid body is capped by a hydrophilic group (-OH vs. the larger carboxy-TEMPO, respectively). Hence, one may assume that, the location and orientation in lipid bilayers should be approximately that of cholesterol in the lipid bilayer. In addition, it has already been shown in other EPR studies that MBP does not insert itself very deeply into the lipid bilayer and that parts of the protein (C1 as well as C8) are also located on the surface [48]. This, in combination with the slightly lower-seated position of cholesterol, should position the spin marker at a depth of the bilayer where interacting MBP should reside. Since in the compositions of 0 % and 35 % cholesterol, no significant differences to the behavior of the next higher percentages could be found, these are not shown in the following EPR experiments for clarity. All following EPR spectroscopic experiments were performed at X-band microwave frequencies (9.4 GHz).

3.4.1. CW EPR

CW EPR spectra of CSOSL added as tracer to LUV samples at room temperature or slightly elevated temperatures show the typical nitroxide three-line pattern spectra with slightly changed (slowed down and anisotropic) rotational mobility (Fig. 5). For spectroscopic comparability, all samples contain the same amount of spin label, independent of the cholesterol content. The nitroxide moiety of CSOSL should be located within the (polar) headgroup region of phospholipids, while the hydrophobic ring system and alkyl chain should line up with the hydrocarbon chains towards the bilayer center. The spectra are characteristic for spin label in lipid bilayers structures [49–51] and there is no clear indication for presence of a second component, i.e. CSOSL reflects location on one defined local environment. The temperature-dependent CW EPR spectra of the spin-labeled cholesterol containing vesicles show that the line shapes change with increasing temperature and are anisotropic. Similar line shapes and a similar effect of temperature can be observed for samples containing LUVs and MBP (Fig. 5b).

The hyperfine coupling of nitroxide spin label depends on the unpaired electron spin density at the nitrogen atom. The apparent hyperfine splitting constant ($a_{iso,app}$), i.e. the line separation between the three lines in Fig. 5 can be seen as a simplified parameter of the hyperfine coupling in the fast, isotropic limit. Non-polar solvents favor the neutral mesomeric structure of NO on the TEMPO derivative with higher spin populations on oxygen, leading to smaller line separations in the CW EPR spectra. The more hydrophobic the spin environment, the smaller the coupling constant. Looking at $a_{iso,app}$ of cholesterol-containing LUVs (Fig. 5a), it is clear that the microenvironment changes its polarity. Independent of the cholesterol content, the general trend is that up to 20 °C $a_{iso,app}$ (taken directly from the EPR spectra) rises, then reaches a

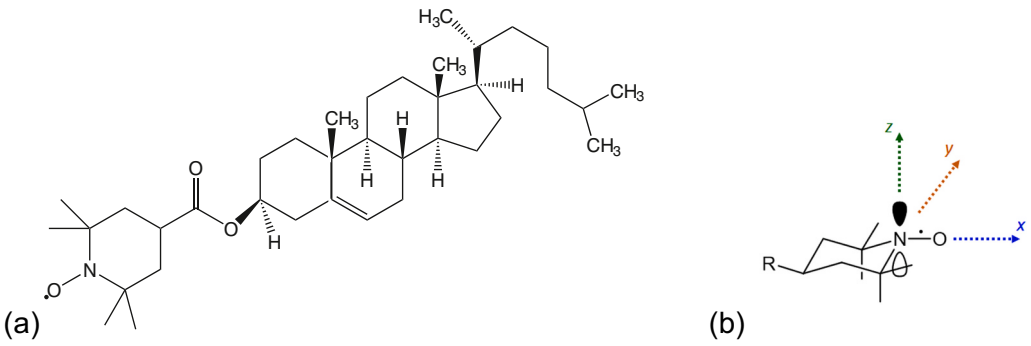

Fig. 4. (a) Chemical structure of spin labeled cholesterol CSOSL. (b) hyperfine splitting (A-) tensor frame of nitroxyl radical (TEMPO, R = H): z-axis parallel to the $2p_z$ orbitals of the nitrogen and oxygen containing the unpaired electron, x-axis along the N—O bond, and y-axis perpendicular to the x,z plane. Euler angle $\beta = 60°$.

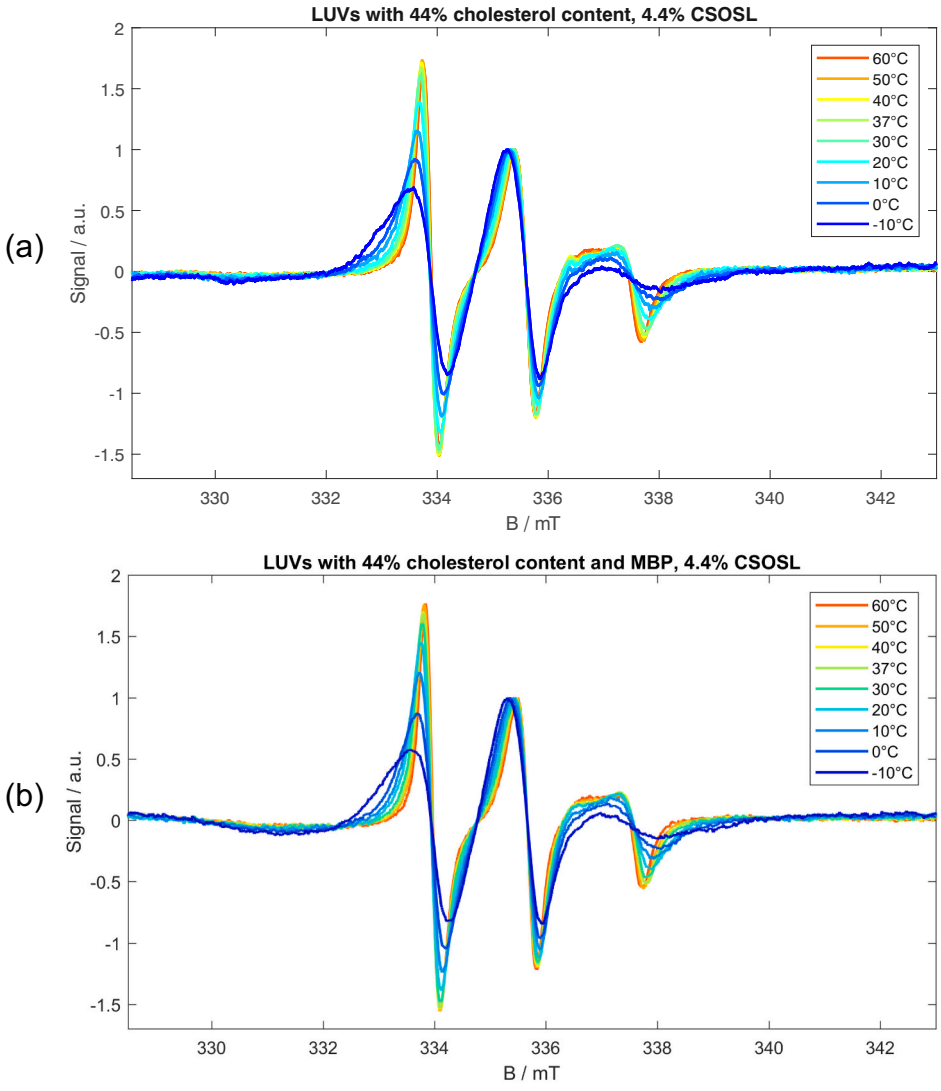

Fig. 5. Temperature series of X-band CW EPR spectra of LUVs containing 44 % cholesterol thereof 4.4 % CSOSL (a) without and (b) with MBP in a HEPES-NaCl buffer normalized to center field peak (each 8 scans, measured at —10 °C to 60 °C, microwave power 5—10 dB, center field 336 mT, sweep width 15 mT, modulation amplitude 0.1 mT).

plateau between 20 °C and 40 °C and then decreases above 40 °C. This is also mirrored in the high field peaks that show migration of the line maxima from lower to higher to lower magnetic field values (Fig. 5). Remarkably, vesicles with 50 % and 60 % cholesterol content seem to offer the most hydrophilic environment at the CSOSL headgroup (highest $a_{iso,app}$ value). Apart from that, there is no order with respect to the cholesterol content. EPR studies of hydrophobicity with the cholestane spin label CSL (see SI for structural formula) in PC bilayers have shown that the hydrophobicity $2A_{zz}$ decreases in the headgroup region with increasing cholesterol content. [40,49] One may explain this by taking into account that by separating the headgroups of the phospholipids the cholesterol induces a packing defect that allows water

molecules to insert deeper into the bilayer, [40,52] leading to a more polar environment for the spin label. In contrast, here, the dependence of cholesterol content could not be observed, just the values for very high (60 %) or low (10 %) cholesterol contents seem to correspond to the respective envelope. But working with a more complex mixture of lipids other properties could affect the polarity. The polarity of the microenvironment of the spin-labeled cholesterol changes with rising temperature and attains a maximum at temperatures of 20—40 °C. Fretten et al. [53] have shown that temperature-induced structural changes occur around the phase transition temperature and are more likely to be a result of lipid-lipid interaction. They also assumed a second structural change at lower temperatures of approx. 10 °C. The temperature-induced changes in the hyperfine coupling constant could therefore be a change in lipid-lipid interaction. If we assume a phase transition temperature of 37 °C (human body temperature and indicated in DLS data) the temperature induced changes in polarity seen here could reflect that in the EPR measurements. In DSC measurements with the native composition of 44 % cholesterol, however, no phase transition temperature could be detected. This is not surprising due to the broadening and less intense heat capacity peak with increasing cholesterol content in lipid mixtures [54]. Hence the change in lipid-lipid interactions could be seen as a highly local phenomenon in the LUV membrane and that is observable locally using the spin labels and EPR.

With MBP, $a_{iso,app}$ follows the same overall pattern of increase-plateau-decrease and 60 % cholesterol containing LUVs offer the most hydrophilic environment for the spin label (Fig. 6b). But the hydrophobicity increases with decreasing cholesterol content in contrast to without MBP. MBP seems to change the polarity of the spin label environment. By partial insertion of MBP into the bilayer, the available space for lipids is reduced and the lipids may reorganize to a more ordered phase. Cholesterol forms condensed rafts [55,56] that are already highly ordered, and therefore cannot reorganize, just fuse and minimize the interface between cholesterol-rich and phospholipid-enriched phases. It is furthermore known from monolayer studies that MBP is not likely to be located in cholesterol-enriched regions, it preferably interacts with the negatively charged lipids PS and PI in the liquid expanded phase surrounding the cholesterol/sphingomyelin rafts, or interacts at the interface region of condensed to liquid expanded phases. [16,23] Effectively, it inserts and reduces the line tension between regions of different chemical composition or order. This can be observed in Fig. S8d, where the differences $\Delta a_{iso,app} = a_{iso,app}(LUV + MBP) - a_{iso,app}(LUV)$ are depicted and show no significant difference in the temperature range of 15 °C to 45 °C. The change in polarity at lower or higher temperatures could be a result of increased creation of stacking defects, allowing stronger water penetration or a change in curvature of the vesicle bilayer [57,58] and therefore a better exposure to the surrounding water, induced by insertion of MBP. LUVs containing 20 % cholesterol and MBP have lower $a_{iso,app}$ values and seem to present a more non-polar/hydrophobic environment for the spin-labeled head groups. This could be due to loss of curvature (more planar bilayers, reduced water-contact) and stability as MBP adheres opposing leaflets together, which correlates well with the maximum contacting area observed in TEM (Fig. 1). The reduced polarity thus indicates that less water can reside between two bilayers.

Simulation of the spectral line shapes using the EasySpin software package [59] allows assessment of the mobility of the spin label. In the molecular frame of the nitroxide moiety, the z-axis is parallel to the (nominal) $2p_z$ orbitals of the nitrogen and oxygen containing the unpaired electron, the x-axis is along the N—O bond, and the y-axis is perpendicular to the x,z plane (Fig. 4b). The x-axis also coincides with the long axis of the cholesterol molecule. All spectra were simulated using the same g-tensor and the diffusion coefficient for rotation perpendicular to the principal axis is fixed at $D_{xx}=D_{yy} = 0.5D_{\perp} = 0.9*10^7\ s^{-1}$ (see all simulations in SI). The nitroxide z-axis is oriented at a fixed Euler angle β (0, β, 0) to the principal rotation axis (II). No dependence of the Euler angles could be observed, as it is the case with other spin-labeled lipids [60]. Since the spin label is not rigidly attached as in CSL (Fig. S8c), the spin label has more freedom for rotation relative to the ring system.

The rotational correlation time τ_{corr} – as a simplified measure of isotropic rotation – is calculated and shown in Fig. 7 in dependence of the temperature and cholesterol content. In both cases, with and without MBP, the rotational motion increases (τ_{corr} value decreases) with temperature until 40 °C, when it reaches a plateau. There is also no significant difference between the samples, i.e., no dependence on cholesterol content. Above 40 °C a maximum of rotational freedom is reached with the above-described differences in polarity. The overall tendency towards faster rotation with higher temperature could be related to the above-mentioned transformation from the crystalline to the fluid phase of the lipid bilayer. This transformation is also dominant when MBP is present. In general, this change in dynamics with increasing temperature has already been observed in various lipid studies [53,61]. As shown by neutron scattering, the molecular dynamics of lipid bilayers are influenced by MBP [61,62]. In a study with DMPA and MBP, it was found that the membrane dynamics outside the plane to the membrane normal (out of plane) on the 1 ns time scale are clearly characterized by spatially limited vertical diffusion movements of the lipids and are significantly strengthened by MBP above the DMPA phase transition (gel to liquid-crystalline) [61]. This could not be observed in the rotation correlation time. Since cholesterol has only a very short alkyl chain and does not interact directly with MBP, this effect is probably not very pronounced when considering CSOSL, which may well sample different

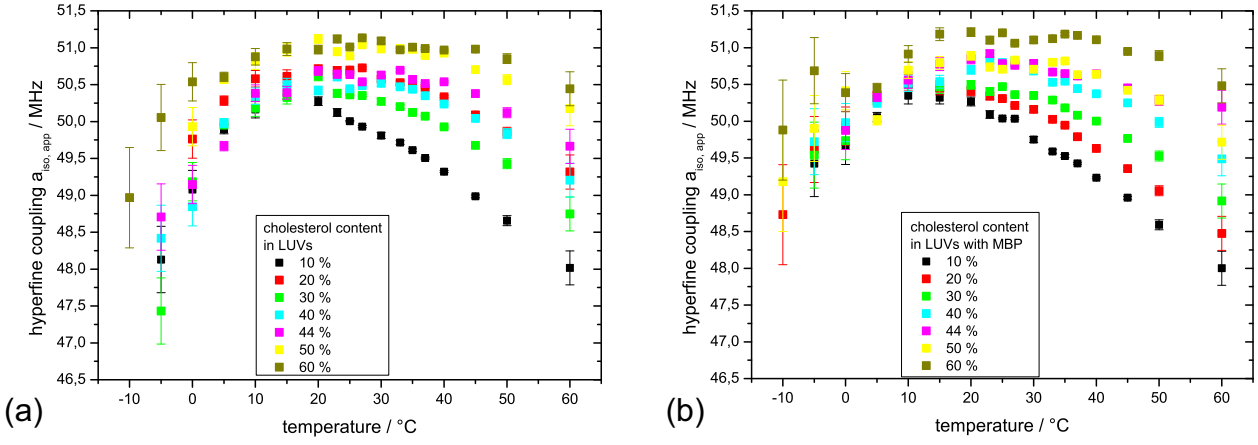

Fig. 6. Apparent isotropic hyperfine coupling constant $a_{iso,app}$ of LUVs with different cholesterol content (a) without and (b) with MBP at varying temperature containing 4.4 % CSOSL. The LUV samples were measured at X-band frequencies in a HEPES-NaCl buffer and with a lipid/protein ratio of 567:1.

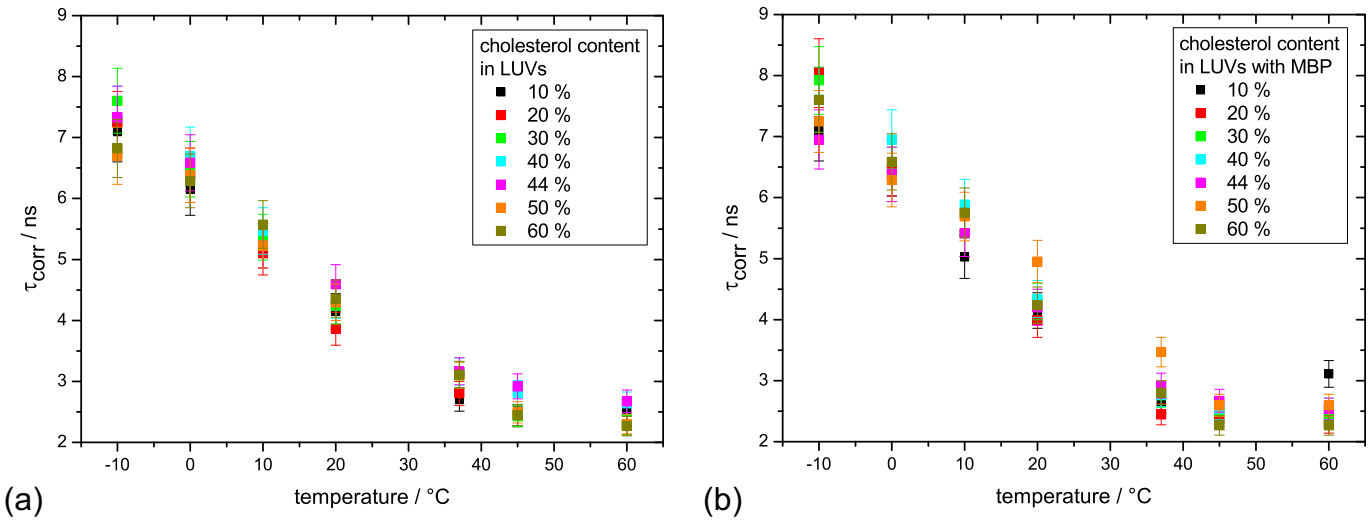

Fig. 7. Rotational correlation time τ_{corr} in dependence of temperature of 4.4 % CSOSL in LUVs with different cholesterol content (a) without and (b) with MBP in a HEPES-NaCl buffer, obtained by simulation of X-band CW EPR spectra.

nanostructured regions than those directly interacting with MBP.

Kusumi et al. [63] have studied the rotational diffusion of the cholestane spin label CSL and showed that CSL is sensitive to the overall order along host alkyl chains, and cholesterol content. Since the molar ratio of the other lipids is constant here and only the amount of cholesterol changes, the influence of the alkyl chains should be negligible. The study considered two independent motions using the method of Israelachvili [51]: rapid axial rotation about the long axis and wobbling of the long axis on a cone. The rotational correlation time is dependent on the diffusion rate D and the Euler angle β. Here, D_{zz} increases with higher temperature, see Fig. 8. Beneath 20 °C, the rotational diffusion coefficient has approximately the same value for samples with and without MBP and is in the slow motion regime. This could be due to the restricted crystalline phase of the lipids dominating the rotational mobility.

Above 20 °C the D_{zz} values in all samples rise more steeply but with different functional dependencies. In all LUVs without MBP from 45 °C and above, most samples have approx. the same rotation around the long axis, only LUVs containing 44 % cholesterol are distinctly different and display a slower rotation of CSOSL (40 % slower). The changes in lipid-lipid interaction indicated by Fretten et al. [53] can here be observed at 10 °C (last value in common) and 37 °C (phase transition temperature, separation of 44 %). As shown before, 44 % cholesterol content has a different behavior than other cholesterol amounts. [23] With MBP, the rotational behavior of the spin label changes above 20 °C when compared to samples without MBP (Fig. 8b). The difference of D_{zz} between samples with and without protein becomes clearer when looking at the difference $\Delta D_{zz} = D_{zz}(LUV + MBP) - D_{zz}(LUV)$ in dependence of the temperature (Fig. S8e). As mentioned before, the rotation of D_{zz} at lower temperature does not change, regardless of the protein content ($\Delta D_{zz} = 0$). At temperatures above 20 °C there is a clear difference observable. In general, samples with MBP show faster rotation at 37 °C. This could be related to the dynamics change in the crystalline phase described above, but this should not significantly affect the in-plane rotation. By interacting with the bilayer, MBP itself occupies space but as suggested before, MBP also could pull together the negatively charged lipids and thereby compact the lipids. [23] The effect would be a partially more highly condensed lipid layer and allowing cholesterol more space for rotation, perhaps needed for non-covalently anchoring in the membrane. As shown in monolayer experiments, 44 % cholesterol content has the highest condensing effect in comparison to lower or higher cholesterol content, resulting in an already highly ordered monolayer that is a good prerequisite for MBP interaction. [23] At 37 °C, the system seems to be in the optimal state for interaction with

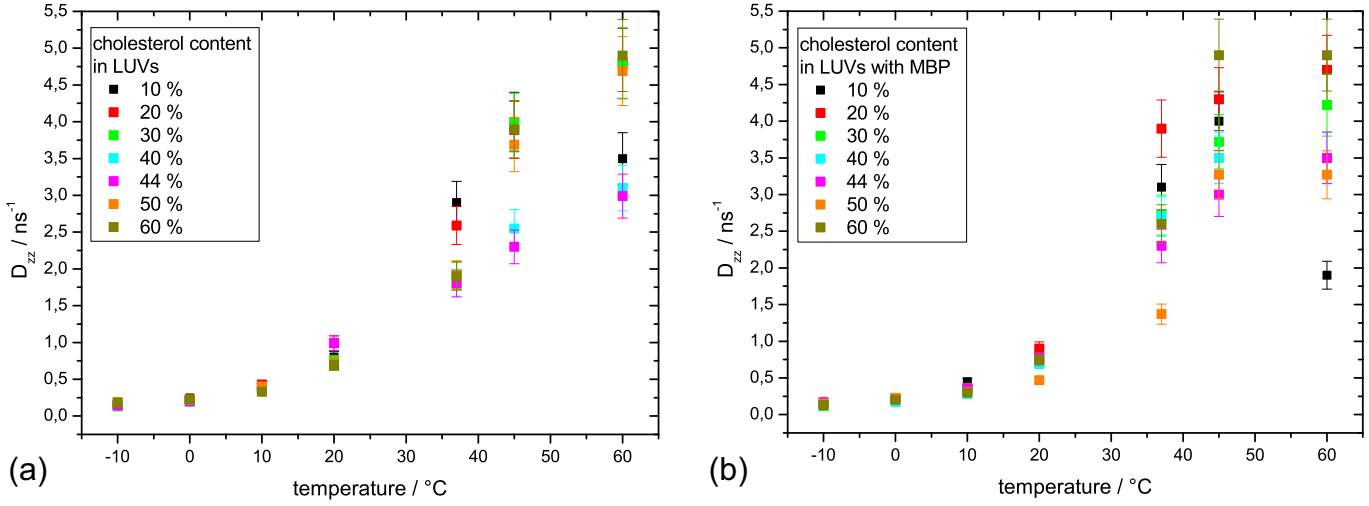

Fig. 8. Rotational diffusion tensor element D_{zz} in dependence of temperature of 4.4 % CSOSL in LUVs with different cholesterol content (a) without and (b) with MBP in a HEPES-NaCl buffer, obtained by simulation of X-band CW EPR spectra.

MBP, as with increasing temperature, the ΔD_{zz} declines, even becoming negative, i.e. the rotation without MBP is faster. With MBP present, the temperature effect on the rotation along the molecular axis seems to have a maximum at body temperature, except samples containing 44 % cholesterol. At temperatures above 37 °C, it can be observed that the D_{zz} rotation of CSOSL in LUVs (44 % cholesterol) with MBP is always 0.6 ns faster than without MBP. This firstly shows again that 44 % cholesterol takes in a special role, and secondly this means that in 44 % cholesterol-containing LUVs the spin-labeled cholesterol molecules increase their rotation with MBP independent of the temperature.

The different rotational rates at 37 °C could result from different initial situations. In LUVs with less cholesterol (10—30 %), the membrane is more fluid at higher temperatures (higher D_{zz}) than with 44 % cholesterol content. From TEM images, we know that the curvature is more planar for 20 %. A planar membrane indicates that the available space for each lipid is cylindrical, and therefore the rotation along the long axis is barely restricted. In a more strongly curved structure (LUV), it is cone-like and the rotation along the x-axis is restricted. In a recent study it was reported that the increase in the thickness of phosphate-to-phosphate (parallel to the bilayer normal) with increasing mol% cholesterol is accompanied by a decrease in the area per lipid [64]. This means that the higher D_{zz} values for LUVs with lower cholesterol content and MBP could result from the available space geometry. While the lipid hydrocarbon chains do not significantly influence the binding affinity, kinetics, or folding of MBP, the dynamic freedom and spatial occupation of the chains define how much MBP can be bound until saturation of the membrane surface is reached [3]. The interaction of MBP with planar or curved surfaces thus also results in a different arrangement of the surrounding lipids, since the depth of penetration and the condensing effect depend on it. The fact that with higher temperatures the ΔD_{zz} value decreases could again indicate the transition into the fluid phase. The lipids move more, require more space, and are further apart, on average. Potentially, this all makes it more unfavorable for MBP to interact with the phospholipids necessary for the secondary structure elements that MBP can form in lipids. In samples with low cholesterol content the high fluidity may counteract MBP binding; in LUVs with high cholesterol content the cholesterol rafts may reduce the phospholipid area. This may lead to MBP losing its anchor and changing it conformation, resulting in a different interaction with the lipid bilayer and the CSOSL experiences a loss in motion freedom. *Trans-Gauche* isomerization can be neglected because of the short alkyl chain in cholesterol. No dependence in Euler angles could be observed as it is by other spin labeled lipids in fluid-bilayer membranes, e.g. lipids spin-labeled at different chain positions. [60]

3.4.2. Pulse EPR: double electron-electron resonance (DEER)

DEER measurements were performed on samples representative for high, medium and low cholesterol contents (60 %, 44 %, and 20 % cholesterol), respectively. Moreover, cholesterol-containing LUVs with and without MBP were studied. The pulse EPR method of DEER records the dipolar modulation signal between unpaired electron spins to obtain structural (distance and potentially angular) information. [65–67] Here, the 4-pulse variant was used at 50 K (further information to experimental setup and measuring technique can be found in the Experimental and SI). In every sample, the CSOSL content (100 μM) was kept identical. The samples were prepared at room temperature (22 °C), mixed with glycerol (20 vol%) acting as cryoprotectant (that does not significantly perturb water structure, see [68]) and then shock frozen. Before each DEER measurement, an electron spin echo (ESE) measurement was carried out in order to determine the frequencies of the observer and pump pulses and to obtain any additional information regarding phase relaxation and nuclear spin modulations. However, due to the signal/noise ratio, no differences could be found between the spectra of the samples (S8g), which is why these are not discussed further.

Fig. 9 shows the dependences $V(t)/V(0)$ against t obtained for CSOSL in LUVs with different cholesterol content with and without the addition of MBP. All time traces reveal no dominant oscillation, which is characteristic for superposition of many dipolar evolution frequencies either indicating a fully homogeneous distribution of spin-spin distances or at least several distances apparently canceling their dipolar oscillations due to their superposition. When inspecting the modulation depths of all time traces of the LUV experiments, a clear dependence of cholesterol content is visible. 44 % cholesterol content shows the deepest modulation depth, 60 % the lowest and 20 % is intermediate between these two. A quantitative measure for the number of spins within the accessible distance range can be extracted from the modulation depth [69]. This means that with 44 % cholesterol content, the distance distribution between the spin labels is such that the spins have their closest approach and highest local (two-dimensional) concentration, resulting in the deepest modulation depth. Again 44 % cholesterol content shows special behavior. LUVs containing 60 % cholesterol show the lowest depth, meaning that fewer spins are in the sensitive distance range. This could result from an increasing average distance between CSOSL molecules because of higher cholesterol content (and identical CSOSL content) or

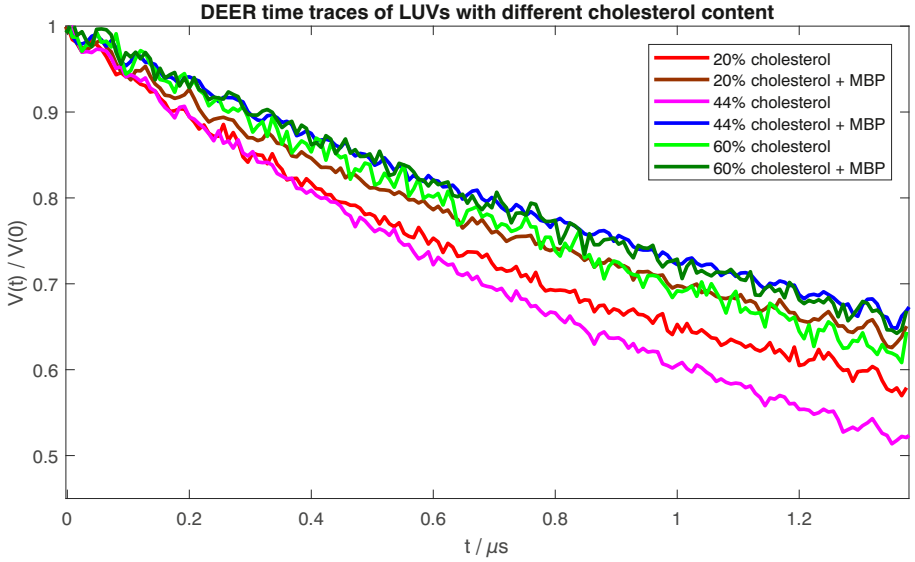

Fig. 9. Background and phase corrected DEER time traces of CSOSL in vesicles with 20 %, 44 % and 60 % cholesterol content with and without MBP at a lipid to protein ratio of 567:1 in a HEPES-NaCl buffer at 50 K (τ_2 = 1,5 μs).

the formation of more cholesterol-enriched domains. [23] With 20 % cholesterol content, the modulation depth has a steep beginning (similar to 44 % cholesterol) but ends in the region of 60 %. This could indicate that within cholesterol-rich domains, locally, the distribution in the 20 % LUVs is similar to that in 44 % LUVs. Yet, the distribution of cholesterol-rich domains may dominate at longer evolution times and it seems that the 20 % LUV samples in this respect resemble the 60 % LUVs. Again, 44 % cholesterol-containing LUVs behave in a special manner and seem to lead to optimized domain size to domain number ratio. Hence, despite no clear difference being observable with the more macroscopic techniques (DLS, TEM), the LUVs with different cholesterol content on a nanoscopic scale of the bilayer membrane display a clear difference.

With MBP all time traces are overlapping with the time trace of 60 % cholesterol content. The modulation depth of 60 % does not change after adding MBP, while those of 20 % and 44 % cholesterol content samples with MBP are reduced. Fewer spins are in the sensitive distance range, suggesting that MBP is incorporated into the bilayer and decreases the available space per lipid and therefore sets apart the spin-labeled cholesterol molecules. But it also indicates that there is some kind of maximum distance because the modulation amplitude in sample with 60 % cholesterol content does not change. MBP has the strongest effect on the LUVs with 44 % cholesterol content, i.e. the difference between the modulation depth without and with MBP is the largest. This could be due to (1) the ratio between SM and cholesterol being optimal, it forms the most compact domains that are necessary for myelin compaction [29]; (2) the fluidity (unsaturated chain content) and rigidity (cholesterol amount) of the bilayer being in perfect balance [29,70]; or/and (3) the structures and line tensions of cholesterol-rich domains and phospholipid-rich phase being optimized to obtain the free energy minimum [39].

4. Conclusion

In this study, we have investigated how the cholesterol content affects LUVs with a lipid composition similar to the cytoplasmic leaflet of myelin and how the simultaneous interaction of these LUV bilayer membranes with myelin basic protein changes LUV behavior and shape. Different experimental techniques were utilized to obtain detailed insights into the microscopic/nanoscopic behavior.

On the more global scale of the LUVs, it was shown by DLS that LUVs containing different cholesterol contents form spherical and uniformly-sized vesicles, and are temperature stable in a range from 0—60 °C. Adding MBP to the LUVs, MBP clearly interacts with the bilayers and bigger aggregates were found in DLS, again indicating the adhesive effect of MBP in the myelin sheath. Interestingly, the aggregation behavior changes at the native 44 % cholesterol content. When MBP is present, clear differences become visible in cryo-TEM concerning the shape and aggregation behavior. With 44 % cholesterol content (native amount) the binding through MBP is more ordered. The vesicles keep their initial round shape and persist an almost regular distance from each other without decreasing the effectiveness of aggregation. One may speculate that these findings reflect the optimization of the myelin sheath with the 44 % cholesterol content. Since the myelin sheath is wrapped around the axon such that the curvature decreases with increasing diameter, it seems that 44 % cholesterol containing LUVs with MBP have the ability to balance the change in diameter and curvature best, maintaining stability, shape and homogeneity. 20 % and 60 % cholesterol containing LUVs seem to act mechanically (at least from the cryo-TEM perspective). Looking at the membrane potential of the slipping plane via the zeta potential no dependence of cholesterol content could be observed, neither without MBP nor with interaction of MBP.

Performing EPR spectroscopy, we were able to obtain information on a specific molecule cholesterol (CSOSL; spin label: carboxy TEMPO) in the cholesterol-rich regions of the bilayers. From the CW EPR the polarity at the spin label was extracted. It is known from previous studies [29,49] that the polarity in the headgroup region increases with increasing cholesterol content. This can just partly be observed here. With MBP the polarity increases with increasing cholesterol content. This means that the polarity changes with interaction of MBP even though MBP does not interact directly with cholesterol. By investigating the rotation rate (D_{zz}), we find that only 44 % cholesterol containing LUVs shows different rotation rates with and without MBP. Studying the modulation depth of time traces of DEER experiments indicate that LUVs with 44 % cholesterol content seem to have the optimal distance and distribution of cholesterol. The same experiments with MBP show that fewer spins are in the DEER-accessible range independent of the cholesterol content, with the biggest effect seen with 44 % cholesterol. Strengthening the theory that MBP reduces the available space in bilayers.

When discussing the relevance of different cholesterol contents in a clinical setting, one may speculate that physiologically the charge variation in MBP (post-translational reduction of positive charges as found in multiple sclerosis) may be a reaction to compensate for the non-ideal/non-native cholesterol content. Of course, this assumes that the lipid composition is the initial, upstream effect, and would coincide with our findings of charge-dependent insertion differences of MBP into monolayers with different sphingomyelin contents [25].

Still more detailed information on the specific interaction of MBP with the bilayer is difficult to obtain. Nevertheless, by using the lipid composition similar to the cytoplasmic leaflet of myelin and a mixture of MBP variants, this model system is closer to the natural system. However, further investigations under more physiological conditions, e.g., by adjusting salt contents or introducing divalent metal ions as zinc or cupper, have to be performed.

It is very clear that the cholesterol content is important for LUV behavior and in particular for the MBP interaction with the myelin-like bilayer. With MBP depending on the cholesterol content, the size, the shape, the aggregation behavior, the stability, and the fluidity of the LUVs changes as well as the rotational motion, the environmental polarity and the distribution of the spin labeled cholesterol. We find that often experiments at 37 °C stand out and in almost every experimental series, the samples containing the native 44 % cholesterol show special behavior or marks the point of change for the measured physical quantity. Although studied in this specific myelin-like system, from a more general and materials science-oriented point of view, we could establish how membrane and vesicle properties depend on cholesterol and/or MBP content, which might be useful generally when specific membrane and vesicle characteristics are sought for.

CRediT authorship contribution statement

Jennica Träger: Methodology, Investigation, Validation, Formal analysis, Data curation, Writing – original draft, Project administration. **Annette Meister:** Validation, Writing – review & editing. **Gerd Hause:** Validation, Writing – review & editing. **George Harauz:** Conceptualization, Writing – review & editing, Funding acquisition. **Dariush Hinderberger:** Conceptualization, Funding acquisition, Resources, Writing – review & editing, Supervision.

Declaration of competing interest

The authors declare the following financial interests/personal relationships which may be considered as potential competing interests: Dariush Hinderberger reports financial support was provided by German Research Foundation. George Harauz reports financial support was provided by Natural Sciences and Engineering Research Council of Canada.

Acknowledgments

This research was funded by the Deutsche Forschungsgemeinschaft

(DFG) under grant number HI 1094/7-1 (DH), the Natural Sciences and Engineering Research Council of Canada (Discovery Grant RG121541 to GH), and the Canada Research Chairs Program (GH). We thank H. Schimm, J. Eisermann and H. Hashemi Haeri for technical assistance and advice. Anja Knorrscheidt (The Lab Lady) we thank for creating the graphical abstract.

Appendix A. Supplementary data

Supplementary data to this article can be found online at https://doi.org/10.1016/j.bbamem.2023.184179.

References

[1] J.K. Kim, F.G. Mastronardi, D.D. Wood, D.M. Lubman, R. Zand, M.A. Moscarello, Multiple Sclerosis, Mol. Cell. Proteomics 2 (2003) 453–462, https://doi.org/10.1074/mcp.M200050-MCP200.
[2] G. Harauz, A.A. Musse, A tale of two citrullines - structural and functional aspects of myelin basic protein deimination in health and disease, Neurochem. Res. 32 (2007) 137–158, https://doi.org/10.1007/s11064-006-9108-9.
[3] A. Raasakka, S. Ruskamo, J. Kowal, R. Barker, A. Baumann, A. Martel, J. Tuusa, M. Myllykoski, J. Bürck, A.S. Ulrich, H. Stahlberg, P. Kursula, Membrane association landscape of myelin basic protein portrays formation of the myelin major dense line, Sci. Rep. 7 (2017), https://doi.org/10.1038/s41598-017-05364-3.
[4] R. Shaharabani, M. Ram-On, R. Avinery, R. Aharoni, R. Arnon, Y. Talmon, R. Beck, Structural transition in myelin membrane as initiator of multiple sclerosis, J. Am. Chem. Soc. 138 (2016) 12159–12165, https://doi.org/10.1021/jacs.6b04826.
[5] R. Shaharabani, M. Ram-On, Y. Talmon, R. Beck, Pathological transitions in myelin membranes driven by environmental and multiple sclerosis conditions, Proc. Natl. Acad. Sci. U. S. A. 115 (2018) 11156–11161, https://doi.org/10.1073/pnas.1804275115.
[6] G. Harauz, N. Ishiyama, C.M.D. Hill, I.R. Bates, D.S. Libich, C. Farès, Myelin basic protein - diverse conformational states of an intrinsically unstructured protein and its roles in myelin assembly and multiple sclerosis, Micron. 35 (2004) 503–542, https://doi.org/10.1016/j.micron.2004.04.005.
[7] A.K. Dunker, I. Silman, V.N. Uversky, J.L. Sussman, Function and structure of inherently disordered proteins, Curr. Opin. Struct. Biol. 18 (2008) 756–764, https://doi.org/10.1016/J.SBI.2008.10.002.
[8] K.A. Vassall, V.V. Bamm, G. Harauz, MyelStones: the executive roles of myelin basic protein in myelin assembly and destabilization in multiple sclerosis, Biochem. J. 472 (2015) 17–32, https://doi.org/10.1042/BJ20150710.
[9] A. Raasakka, P. Kursula, Flexible players within the sheaths: the intrinsically disordered proteins of myelin in health and disease, Cells. 9 (2020) 470, https://doi.org/10.3390/cells9020470.
[10] C. Zhang, A.K. Walker, R. Zand, M.A. Moscarello, J.M. Yan, P.C. Andrews, Myelin basic protein undergoes a broader range of modifications in mammals than in lower vertebrates, J. Proteome Res. 11 (2012) 4791–4802, https://doi.org/10.1021/pr201196e.
[11] B. Ohler, K. Graf, R. Bragg, T. Lemons, R. Coe, C. Genain, J. Israelachvili, C. Husted, Role of lipid interactions in autoimmune demyelination, Biochim. Biophys. Acta - Mol. Basis Dis. 1688 (2004) 10–17, https://doi.org/10.1016/j.bbadis.2003.10.001.
[12] M.A. Moscarello, D.D. Wood, C. Ackerley, C. Boulias, Myelin in multiple sclerosis is developmentally immature, J. Clin. Invest. 94 (1994) 146–154, https://doi.org/10.1172/JCI117300.
[13] K.A. Vassall, V.V. Bamm, A.D. Jenkins, C.J. Velte, D.R. Kattnig, J.M. Boggs, D. Hinderberger, G. Harauz, Substitutions mimicking deimination and phosphorylation of 18.5-kDa myelin basic protein exert local structural effects that subtly influence its global folding, Biochim. Biophys. Acta Biomembr. 1858 (2016) 1262–1277, https://doi.org/10.1016/j.bbamem.2016.02.024.
[14] M.A.M. Ahmed, M. De Avila, E. Polverini, K. Bessonov, V.V. Bamm, G. Harauz, Solution nuclear magnetic resonance structure and molecular dynamics simulations of a murine 18.5 kDa myelin basic protein segment (S72–S107) in association with Dodecylphosphocholine micelles, Biochemistry. 51 (2012) 7475–7487, https://doi.org/10.1021/bi300998x.
[15] P.D. Boggs, M.A. Moscarello, Structural organization of myelin: role of lipid protein interactions determined in model systems, in: O.H. Jost, P.C. Griffith (Eds.), Lipid-Protein Interact, Wiley-Interscience, New York, 1982, pp. 1–51.
[16] K. Widder, J. Träger, A. Kerth, G. Harauz, D. Hinderberger, Interaction of myelin basic protein with myelin-like lipid monolayers at air−water Interface, Langmuir. 34 (2018) 6095–6108, https://doi.org/10.1021/acs.langmuir.8b00321.
[17] T.H. Bayburt, S.G. Sligar, Membrane protein assembly into Nanodiscs, FEBS Lett. 584 (2010) 1721–1727, https://doi.org/10.1016/j.febslet.2009.10.024.
[18] M. Hoffmann, D. Haselberger, T. Hofmann, L. Müller, K. Janson, A. Meister, M. Das, C. Vargas, S. Keller, P.L. Kastritis, C. Schmidt, D. Hinderberger, Nanoscale model system for the human myelin sheath, Biomacromolecules. 22 (2021) 3901–3912, https://doi.org/10.1021/acs.biomac.1c00714.
[19] C.D. Pointer-Keenan, D.-K. Lee, K. Hallok, A. Tan, R. Zand, A. Ramamoorthy, Investigation of the interaction of myelin basic protein with phospholipid bilayers using solid-state NMR spectroscopy, Chem. Phys. Lipids 132 (2004) 47–54, https://doi.org/10.1016/j.chemphyslip.2004.09.004.
[20] I.R. Bates, P. Matharu, N. Ishiyama, D. Rochon, D.D. Wood, E. Polverini, M. A. Moscarello, N.J. Viner, G. Harauz, Characterization of a recombinant murine 18.5-kDa myelin basic protein, Protein Expr. Purif. 20 (2000) 285–299, https://doi.org/10.1006/prep.2000.1307.
[21] A. Raasakka, S. Ruskamo, J. Kowal, R. Barker, A. Baumann, A. Martel, J. Tuusa, M. Myllykoski, J. Bürck, A.S. Ulrich, H. Stahlberg, P. Kursula, Membrane association landscape of myelin basic protein portrays formation of the myelin major dense line, Sci. Rep. 7 (2017) 1–18, https://doi.org/10.1038/s41598-017-05364-3.
[22] K. Meller, Cryo-electron microscopy of vitrified nerve myelin, Cell Tissue Res. 262 (1990) 59–66, https://doi.org/10.1007/BF00327746.
[23] J. Träger, K. Widder, A. Kerth, G. Harauz, D. Hinderberger, Effect of cholesterol and myelin basic protein (MBP) content on lipid monolayers mimicking the cytoplasmic membrane of myelin, Cells. 9 (2020) 529, https://doi.org/10.3390/cells9030529.
[24] H. Inouye, D.A. Kirschner, Membrane interactions in nerve myelin: II. Determination of surface charge from biochemical data, Biophys. J. 53 (1988) 247–260, https://doi.org/10.1016/S0006-3495(88)83086-8.
[25] K. Widder, G. Harauz, D. Hinderberger, Myelin basic protein (MBP) charge variants show different sphingomyelin-mediated interactions with myelin-like lipid monolayers, Biochim. Biophys. Acta Biomembr. 1862 (2020), 183077, https://doi.org/10.1016/J.BBAMEM.2019.183077.
[26] K. Widder, G. Harauz, D. Hinderberger, Charge-dependent myelin basic protein – sphingomyelin interactions in myelin-like lipid monolayers, (n.d.) 1–13.
[27] N.P. Franks, Structural analysis of hydrated egg lecithin and cholesterol bilayers I. X-ray diffraction, J. Mol. Biol. 100 (1976) 345–358.
[28] D.L. Worcester, N.P. Franks, Structural analysis of hydrated egg lecithin and cholesterol bilayers II. Neutron diffraction, J. Mol. Biol. 100 (1976) 359–378, https://doi.org/10.1016/S0022-2836(76)80068-X.
[29] W.K. Subczynski, M. Pasenkiewicz-Gierula, J. Widomska, L. Mainali, M. Raguz, High cholesterol/low cholesterol: effects in biological membranes: a review, Cell Biochem. Biophys. 75 (2017) 369–385, https://doi.org/10.1007/s12013-017-0792-7.
[30] P.L. Yeagle, W.C. Hutton, C.H. Huang, R.B. Martin, Phospholipid head-group conformations, Intermolecular Interactions and Cholesterol Effects, Biochemistry. 16 (1977) 4344–4349, https://doi.org/10.1021/bi00639a003.
[31] A. Radhakrishnan, T.G. Anderson, H.M. McConnell, Condensed complexes, rafts, and the chemical activity of cholesterol in membranes, Proc. Natl. Acad. Sci. U. S. A. 97 (2000) 12422–12427, https://doi.org/10.1073/pnas.220418097.
[32] J.R. Silvius, Role of cholesterol in lipid raft formation: lessons from lipid model systems, Biochim. Biophys. Acta Biomembr. 1610 (2003) 174–183, https://doi.org/10.1016/S0005-2736(03)00016-6.
[33] T. Hauenschild, J. Reichenwallner, V. Enkelmann, D. Hinderberger, Characterizing active pharmaceutical ingredient binding to human serum albumin by spin-labeling and EPR spectroscopy, Chem. - A Eur. J. 22 (2016) 12825–12838, https://doi.org/10.1002/chem.201601810.
[34] V.V. Bamm, D.K. Lanthier, E.L. Stephenson, G.S.T. Smith, G. Harauz, In vitro study of the direct effect of extracellular hemoglobin on myelin components, Biochim. Biophys. Acta - Mol. Basis Dis. 2015 (1852) 92–103, https://doi.org/10.1016/j.bbadis.2014.10.009.
[35] D.R. Kattnig, T. Bund, J.M. Boggs, G. Harauz, D. Hinderberger, Lateral self-assembly of 18.5-kDa myelin basic protein (MBP) charge component-C1 on membranes, Biochim. Biophys. Acta Biomembr. 1818 (2012) 2636–2647, https://doi.org/10.1016/j.bbamem.2012.06.010.
[36] E. Jo, J.M. Boggs, Aggregation of acidic lipid vesicles by myelin basic protein: dependence on potassium concentration, Biochemistry. 34 (1995) 13705–13716, https://doi.org/10.1021/bi00041a053.
[37] M. Raguz, S.N. Kumar, M. Zareba, N. Ilic, L. Mainali, W.K. Subczynski, Confocal microscopy confirmed that in phosphatidylcholine Giant Unilamellar vesicles with very high cholesterol content pure cholesterol bilayer domains form, Cell Biochem. Biophys. 77 (2019) 309–317, https://doi.org/10.1007/s12013-019-00889-y.
[38] Y. Min, K. Kristiansen, J.M. Boggs, C. Husted, J.A. Zasadzinski, J. Israelachvili, Interaction forces and adhesion of supported myelin lipid bilayers modulated by myelin basic protein, Proc. Natl. Acad. Sci. U. S. A. 106 (2009) 3154–3159, https://doi.org/10.1073/pnas.0813110106.
[39] W.K. Subczynski, A. Kusumi, Dynamics of raft molecules in the cell and artificial membranes: approaches by pulse EPR spin labeling and single molecule optical microscopy, Biochim. Biophys. Acta Biomembr. 1610 (2003) 231–243, https://doi.org/10.1016/S0005-2736(03)00021-X.
[40] W.K. Subczynski, A. Wisniewska, W.K. Subczynski, A. Wisniewska, J.J. Yin, J. S. Hyde, A. Kusumi, Hydrophobic barriers of lipid bilayer membranes formed by reduction of water penetration by alkyl chain unsaturation and cholesterol, Biochemistry. 33 (1994) 7670–7681, https://doi.org/10.1021/bi00190a022.
[41] T. Heimburg, Thermal Biophysics of Membranes, Tutorials in Biophysics, John Wiley & Sons, 2008.
[42] L.K. Buehler, Cell Membranes, Garland Science, Taylor & Francis Group, New York, 2016.
[43] T. Heimburg, Thermal biophysics of membranes, Wiley (2007), https://doi.org/10.1002/9783527611591.
[44] S. Garcia-Manyes, G. Oncins, F. Sanz, Effect of temperature on the Nanomechanics of lipid bilayers studied by force spectroscopy, Biophys. J. 89 (2005) 4261–4274, https://doi.org/10.1529/biophysj.105.065581.
[45] M. Kaszuba, J. Corbett, F.M. Watson, A. Jones, High-concentration zeta potential measurements using light-scattering techniques, Philos. Trans. R. Soc. A Math. Phys. Eng. Sci. 368 (2010) 4439–4451, https://doi.org/10.1098/rsta.2010.0175.

[46] C. Bellmann, A. Caspari, C. Moitzi, F. Babick, Dynamische und elektrophoretische Lichtstreuung, Anton Paar, 2018.
[47] B.J. Kirby, E.F. Hasselbrink, Zeta potential of microfluidic substrates: 1. Theory, experimental techniques, and effects on separations, Electrophoresis. 25 (2004) 187–202, https://doi.org/10.1002/elps.200305754.
[48] I.R. Bates, J.M. Boggs, J.B. Feix, G. Harauz, Membrane-anchoring and charge effects in the interaction of myelin basic protein with lipid bilayers studied by site-directed spin labeling, J. Biol. Chem. 278 (2003) 29041–29047, https://doi.org/10.1074/jbc.M302766200.
[49] M. Raguz, L. Mainali, J. Widomska, W.K. Subczynski, Using spin-label electron paramagnetic resonance (EPR) to discriminate and characterize the cholesterol bilayer domain, Chem. Phys. Lipids 164 (2011) 819–829, https://doi.org/10.1016/j.chemphyslip.2011.08.001.
[50] L.J. Berliner, SpinLabeling I, Theory and Applications, Academic Press, New York, 1976.
[51] J. Israelachvili, J. Sjösten, L.E.G. Eriksson, M. Ehrström, A. Gräslund, A. Ehrenberg, ESR spectral analysis of the molecular motion of spin labels in lipid bilayers and membranes based on a model in terms of two angular motional parameters and rotational correlation times, Biochim. Biophys. Acta Biomembr. 382 (1975) 125–141, https://doi.org/10.1016/0005-2736(75)90171-6.
[52] W.K. Subczynski, J. Widomska, J.B. Feix, Their influence on chemical reactions in a membrane environment, Free Radic. Biol. Med. 46 (2010) 707–718, https://doi.org/10.1016/j.freeradbiomed.2008.11.024.
[53] P. Fretten, S.J. Morris, A. Watts, D. Marsh, Lipid-lipid and lipid-protein interactions in chromaffin granule membranes, A spin label ESR study, BBA - Biomembr. 598 (1980) 247–259, https://doi.org/10.1016/0005-2736(80)90003-6.
[54] W.I. C., G.G. Shipley, Sphingomyelin-lecithin bilayers and their interaction with cholesterol, Biochemistry. 18 (1979) 1717–1722.
[55] J.B. Leathes, Croonian lectures On the role of fats in vital phenomena, Lancet. 205 (1925) 957–962, https://doi.org/10.1016/S0140-6736(01)22402-7.
[56] H.M. McConnell, A. Radhakrishnan, Condensed complexes of cholesterol and phospholipids, Biochim. Biophys. Acta Biomembr. 1610 (2003) 159–173, https://doi.org/10.1016/S0005-2736(03)00015-4.
[57] M. Simunovic, G.A. Voth, A. Callan-Jones, P. Bassereau, When physics takes over: BAR proteins and membrane curvature, Trends Cell Biol. 25 (2015) 780–792, https://doi.org/10.1016/j.tcb.2015.09.005.
[58] B. Sorre, A. Callan-Jones, J.-B. Manneville, P. Nassoy, J.-F. Joanny, J. Prost, B. Goud, P. Bassereau, Curvature-driven lipid sorting needs proximity to a demixing point and is aided by proteins, Proc. Natl. Acad. Sci. 106 (2009) 5622–5626, https://doi.org/10.1073/pnas.0811243106.
[59] S. Stoll, A. Schweiger, EasySpin, a comprehensive software package for spectral simulation and analysis in EPR, J. Magn. Reson. 178 (2006) 42–55, https://doi.org/10.1016/j.jmr.2005.08.013.
[60] D. Marsh, Distinct populations in spin-label EPR spectra from Nitroxides, J. Phys. Chem. B 122 (2018) 6129–6133, https://doi.org/10.1021/acs.jpcb.7b11294.
[61] F. Natali, A. Relini, A. Gliozzi, R. Rolandi, P. Cavatorta, A. Deriu, A. Fasano, P. Riccio, Protein–membrane interaction: effect of myelin basic protein on the dynamics of oriented lipids, Chem. Phys. 292 (2003) 455–464, https://doi.org/10.1016/S0301-0104(03)00255-6.
[62] W. Knoll, J. Peters, P. Kursula, Y. Gerelli, J. Ollivier, B. Demé, M. Telling, E. Kemner, F. Natali, Structural and dynamical properties of reconstituted myelin sheaths in the presence of myelin proteins MBP and P2 studied by neutron scattering, Soft Matter 10 (2014) 519–529, https://doi.org/10.1039/C3SM51393A.
[63] A. Kusumi, M. Pasenkiewicz-gierula, Rotational diffusion of a steroid molecule in phosphatidylcholine membranes: effects of alkyl chain length, unsaturation, and cholesterol as studied by a spin-label method, Biochemistry. 27 (1988) 4407–4415, https://doi.org/10.1021/bi00412a030.
[64] N. Kučerka, J. Pencer, M.-P. Nieh, J. Katsaras, Influence of cholesterol on the bilayer properties of monounsaturated phosphatidylcholine unilamellar vesicles, Eur. Phys. J. E. 23 (2007) 247–254, https://doi.org/10.1140/epje/i2007-10202-8.
[65] G. Jeschke, Y. Polyhach, Distance measurements on spin-labelled biomacromolecules by pulsed electron paramagnetic resonance, Phys. Chem. Chem. Phys. 9 (2007) 1895–1910, https://doi.org/10.1039/b614920k.
[66] A.D. Milov, A.B. Ponomarev, Y.D. Tsvetkov, Electron-electron double resonance in electron spin echo: model biradical systems and the sensitized photolysis of decalin, Chem. Phys. Lett. 110 (1984) 67–72, https://doi.org/10.1016/0009-2614(84)80148-7.
[67] G. Jeschke, DEER distance measurements on proteins, Annu. Rev. Phys. Chem. 63 (2012) 419–446, https://doi.org/10.1146/annurev-physchem-032511-143716.
[68] J. Hunold, J. Eisermann, M. Brehm, D. Hinderberger, Characterization of aqueous lower-polarity solvation shells around amphiphilic 2,2,6,6-Tetramethylpiperidine-1-oxyl radicals in water, J. Phys. Chem. B 124 (2020) 8601–8609, https://doi.org/10.1021/acs.jpcb.0c04863.
[69] G. Jeschke, G. Panek, A. Godt, A. Bender, H. Paulsen, Data analysis procedures for pulse ELDOR measurements of broad distance distributions, Appl. Magn. Reson. 26 (2004) 223–244, https://doi.org/10.1007/BF03166574.
[70] T. Róg, M. Pasenkiewicz-Gierula, Cholesterol effects on a mixed-chain phosphatidylcholine bilayer: a molecular dynamics simulation study, Biochimie. 88 (2006) 449–460, https://doi.org/10.1016/j.biochi.2005.10.005.